

## Research Article

# Characterization of the Dynamic Imbibition Displacement Mechanism in Tight Sandstone Reservoirs Using the NMR Technique

Liangbin Dou <sup>1,2,3</sup>, Min Yang,<sup>4</sup> Hui Gao,<sup>1,2</sup> Dongxing Jiang,<sup>5</sup> and Chenglu Liu<sup>1,2</sup>

<sup>1</sup>School of Petroleum Engineering, Xi'an Shiyou University, Xi'an 710065, China

<sup>2</sup>Engineering Research Center of Development and Management for Low to Ultra-Low Permeability Oil & Gas Reservoirs in West China, Ministry of Education, Xi'an 710065, China

<sup>3</sup>State Key Laboratory of Petroleum Resources and Prospecting, China University of Petroleum, Beijing 102249, China

<sup>4</sup>Department of Chemical and Petroleum Engineering, University of Calgary, Calgary, AB, Canada T2N 1N4

<sup>5</sup>CNPC Greatwall Drilling Company, Chaoyang, Beijing 100101, China

Correspondence should be addressed to Liangbin Dou; 77129dou@163.com

Received 11 May 2020; Revised 16 June 2020; Accepted 27 November 2020; Published 16 December 2020

Academic Editor: Reza Rezaee

Copyright © 2020 Liangbin Dou et al. This is an open access article distributed under the Creative Commons Attribution License, which permits unrestricted use, distribution, and reproduction in any medium, provided the original work is properly cited.

An experimental technique is developed to investigate the dynamic imbibition displacement mechanism in tight sandstone formations of the Yanchang group of the Ordos basin. By combining the dynamic imbibition core flooding experiments and NMR technique, the effects of the injection volume and rate on displacement efficiency are investigated. Moreover, the displacement efficiency of dynamic imbibition is compared with that of static imbibition. This study gains insights into the micromechanisms of dynamic imbibition in tight sandstone formations. It is found that the relative displacement efficiency of dynamic imbibition increases with the increase of injection volume. But the increment amplitude decreases with the increase of injection volume. With the same injection volume, the core displacement efficiency of dynamic imbibition with high permeability is obviously improved. However, the core displacement efficiency decreases rapidly with the increase of injection volume. Optimal injection volumes are recommended for tight sandstone formations with different permeabilities. With the increase of the displacement rate, the core displacement efficiency of dynamic imbibition shows a trend of first rising and then declining. There exists an optimal displacement rate in dynamic imbibition displacement, and the optimal displacement rate almost linearly increases with the increase of core permeability. The static imbibition displacement efficiency increases with the increase of soaking time, but the increment amplitude slows down obviously. The displacement efficiency of static imbibition in small pores is higher than that of dynamic imbibition. The displacement efficiency of dynamic imbibition in large pores or microcracks is significantly higher than that of static imbibition. This study provides theoretical support for the optimization and improvement of the waterflooding recovery process in tight sandstone reservoirs.

## 1. Introduction

Tight oil is a key area of global unconventional oil development [1]. Unconventional tight oil and gas resources in China are widely distributed and have great development potential [2, 3]. Tight oil and gas resources are found in the Triassic strata of the Ordos basin, Permian strata of the Junggar basin, Cretaceous strata of the Songliao basin, Paleogene strata of the Bohai-Bay basin, and other strata, which have

broad prospects of exploration and development [4]. The tight oil in the Ordos basin is a typical representative of the tight oil resources of continental sedimentation in China. However, compared with the marine tight oil in North America [5–7], there are various types of pores and throats in the tight sandstone reservoir of the Ordos basin. Moreover, the pores and throats are small and widely distributed, with developed microcracks and strong heterogeneity [8]. This results in difficulties in water injection, serious water

breakthrough and out, and low oil recovery in tight oil development. It is of great importance to take advantage of imbibition to improve waterflooding performance.

Imbibition, as an important displacement mechanism in ultralow-permeability reservoirs, has been widely investigated by a large number of scholars [9–23]. Extensive experimental and theoretical studies were carried out to investigate the effect of imbibition on oil recovery and establish classical imbibition models. Spontaneous imbibition experiments were conducted to investigate the ultimate oil recovery, pore structure, and relative permeability curve related to imbibition, further confirming the dominant parameters of imbibition. In addition, some scholars [24–28] have studied the effects of surfactants and other additives on imbibition displacement. With the development of shale oil, the study of imbibition displacement has been shifted from tight sandstone/carbonate reservoirs to shale oil reservoirs. Kuila et al. [29] found that water could be imbibed into almost all nanopores of shale. Later, some scholars [30–34] carried out experiments to study the imbibition displacement mechanism in shale oil reservoirs and analyzed its feasibility. They examined the effects of surfactant and pH value of suction liquid on spontaneous imbibition recovery.

Compared with static imbibition, dynamic imbibition considers the effect of fluid flow in the matrix and fracture on imbibition displacement in the tight reservoir development. Experimental studies on dynamic imbibition [35, 36] have been carried out. They proved the existence of a critical flow rate in the process of imbibition displacement. When the flow rate is higher than the critical flow rate, water breakthrough tends to occur. A corresponding numerical model was developed to capture this phenomenon. Pooladi-Darvish and Firoozabadi [37] analyzed the difference of counter-current imbibition and cocurrent imbibition after water breakthrough in the cores with different permeabilities. Some scholars [28, 38–42] have studied the effects of core wettability, initial water saturation, interfacial tension (IFT), fluid viscosity ratio, soaking time, and permeability on dynamic imbibition. Hammond and Unsal [43] simulated and developed the correlation between the displacement pressure and the imbibition rate during the dynamic imbibition process. Sharma et al. [44] quantitatively evaluated the effects of the flow rate and viscosity ratio on dynamic imbibition displacement. They established a scaling model of dynamic imbibition with the consideration of both the capillary and viscous forces. Qiao et al. [45] and Andersen et al. [46] studied the effect of viscous coupling on the efficiency of dynamic imbibition displacement.

Previous studies mainly applied the conventional core flooding setup to investigate the effect of dynamic imbibition on oil recovery and displacement efficiency. However, the real-time oil-water distribution in different pore-throat-fracture systems cannot be characterized quantitatively during the dynamic imbibition with conventional experiments. Although some scholars have studied the effect of the injection rate on dynamic imbibition, few studies have been done to investigate the relationship between the critical (optimal) injection rate and the core permeability. The total injection volume is very important for cost control and optimization

of water injection. Previous studies on the effect of injection volume on the efficiency of dynamic imbibition displacement are also lacking. Moreover, the comparison of oil and water distribution in pore-throat-fracture systems between static and dynamic imbibition has not been reported. The field application conditions of imbibition recovery in tight reservoirs are still not clear.

In this work, an experimental technique is developed to investigate the real-time distribution of oil and water in pore-throat-fracture systems using tight sandstone cores with various permeabilities in the Ordos basin. The effect of the displacement rate and volume on oil-water distribution in the core microstructure is well clarified. A correlation is developed to represent the relationship between the displacement rate, displacement volume, and core permeability. In addition, the differences between static and dynamic imbibition on imbibition displacement are quantitatively evaluated. This study provides a theoretical foundation for enhancing oil recovery in tight sandstone reservoirs.

## 2. Experimental Section

**2.1. Core Samples and Fluids.** The cores used in the experiments are from tight sandstone formations of the Yanchang group in the Ordos basin. The porosity and permeability are low, but microcracks are well developed. Based on the FE-SEM (FEI Quanta200F) and thin section petrography (TSP) technique tests for four samples shown in Figure 1, it is found that types of pores of tight sandstone in the Yanchang group are mainly intergranular pores, followed by feldspar dissolved pores and debris dissolved pores. The core properties are shown in Table 1. The porosity ranges from 8.29% to 12.36%, and the permeability ranges from 0.138 to 2.451 mD. Synthetic formation water in the target reservoir is used in the experiments. The water used in the experiments is the synthetic formation water in the target reservoir block (water type is  $\text{CaCl}_2$ , salinity is about 18000 mg/l, and viscosity and density at 50°C are 0.523 mPa·s and 1.02 g/cm<sup>3</sup>, respectively). The fluorocarbon oil is used in the experiments (viscosity and density at 50°C are 3.67 mPa·s and 0.82 g/cm<sup>3</sup>, respectively). The viscosity and density are almost equivalent to the formation crude oil. Fluorocarbon oil is able to shield the signal of crude oil in NMR because it does not contain hydrogen. The measured IFT between synthetic formation water and fluorocarbon oil is 12.15 mN/m using an interface tensiometer. In addition, the contact angles of different cores in oil/water/core systems were measured.

**2.2. Experimental Setups.** In this experiment, a constant rate and constant pressure pump (ISCO-500D, USA) is used to control the displacement rate and pressure. The confining pressure can be controlled by injecting fluorocarbon oil with a manual pump, and the maximum confining pressure can reach 20 MPa. The test temperature is controlled by the incubator to maintain the formation temperature. The NMR setup (Niumag Corporation, China) is used to measure the  $T_2$  spectrum of synthetic formation water at various experimental conditions. In addition, the experimental setups also include transfer cylinders in which the brine is injected into

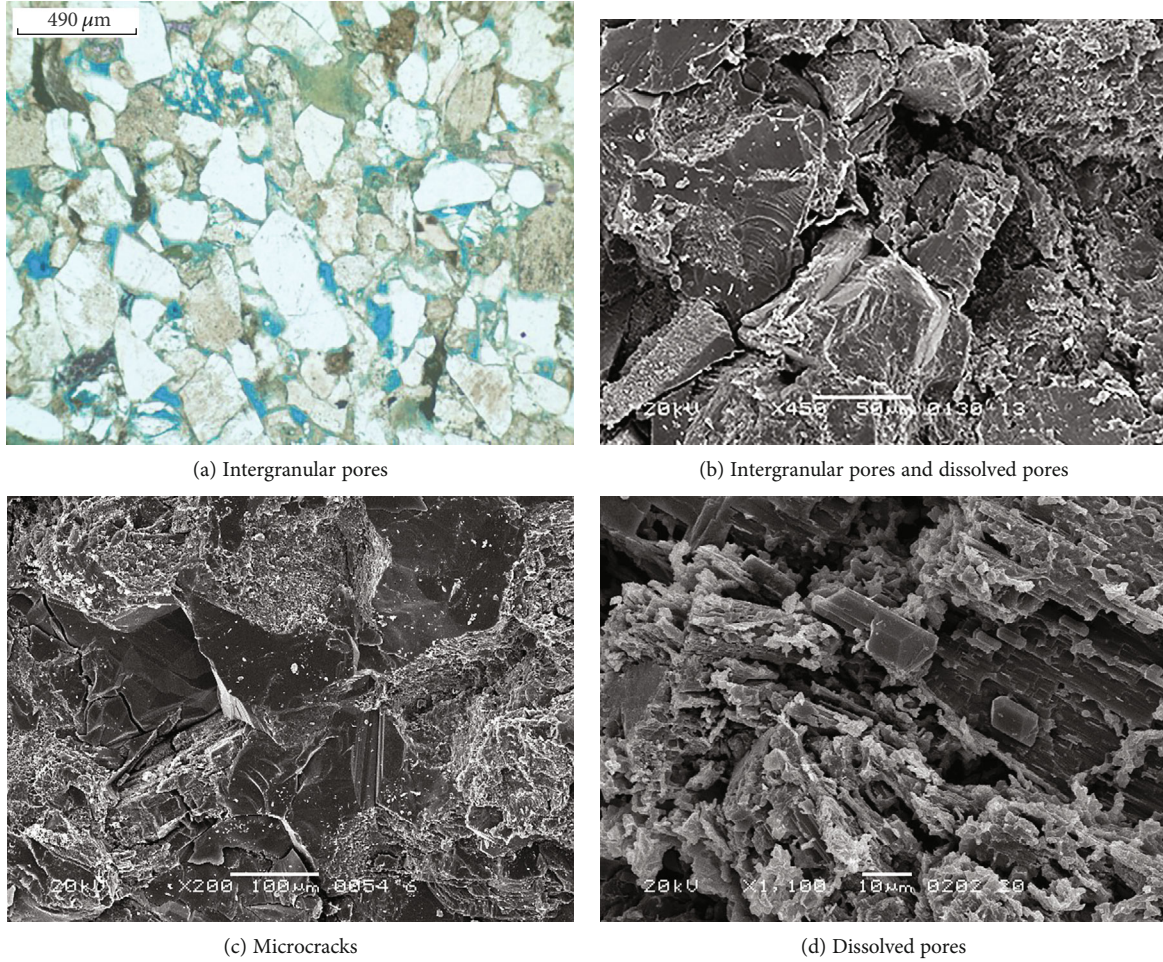


FIGURE 1: The pore types of the Yanchang group tight sandstone samples.

TABLE 1: Properties of experimental cores.

Sample no.	Diameter (mm)	Length (mm)	Porosity (%)	Permeability (mD)	Contact angle (°)
H-3	25.0	43.6	12.36	2.451	46.5
H-7	25.1	42.1	8.29	0.138	43.8
H-15	25.1	42.8	9.36	0.281	37.8
H-21	25.0	44.2	11.32	1.213	51.6

core samples and a core holder which is made of PEEK materials with no hydrogen.

The NMR instrument includes a magnetic body, radiofrequency emitter, and data collection system. The basic parameters of NMR measurements are set. The waiting time and echo time are 5 s and 0.25 ms, respectively. The scanning number and echo number are 16 and 1024, respectively. It was noted that fluorocarbon oil without hydrogen signals does not affect the NMR response. As a result, there is no effect on the measurement of the NMR  $T_2$  spectrum for brine.

2.3. *Experimental Procedures.* Figure 2 presents the schematic diagram of the dynamic imbibition displacement experiment

using the low-field NMR technique. The test temperature is 50°C. The experimental procedures are summarized as follows:

- (1) Place the core in an extraction vessel with a volume ratio of benzene to alcohol of 1:3 to wash the oil. Heat the core to 105°C in an incubator after washing oil and maintain the temperature for 48 h. Then, take out the core and measure the dry weight and dimensions of the core
- (2) Due to the small pore radius of the tight reservoir, conventional vacuum saturation cannot make the core pore completely saturated with water. So, the core is placed into the core holder, and a high-pressure displacement device is used to inject synthetic formation water into the core. When the produced liquid is about 5 PV, the NMR spectrum is measured for the first time. The injection is continued until the production reaches 10 PV. The NMR spectrum is measured again. When there is no significant difference between the two NMR spectra, it can be concluded that the core pore is completely saturated with formation water

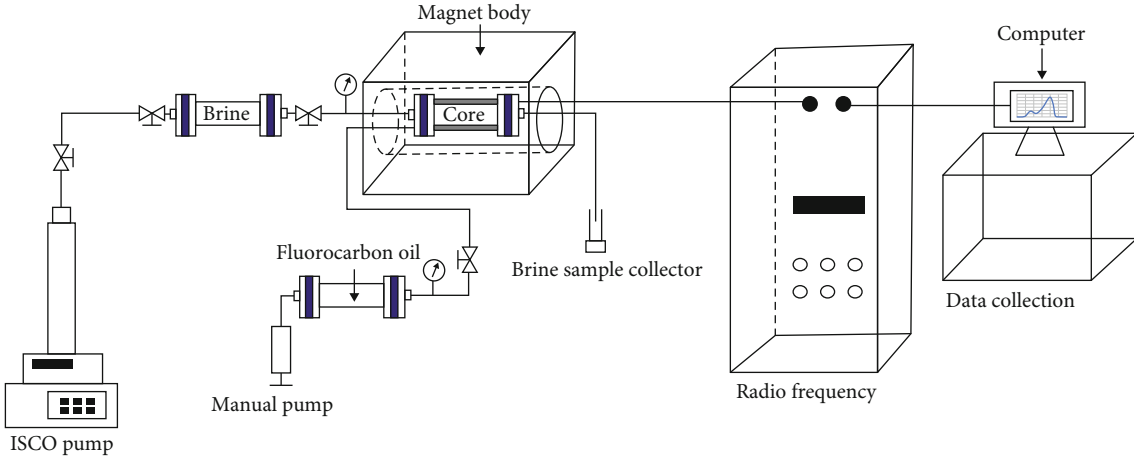


FIGURE 2: Schematic diagram of the dynamic imbibition displacement experiment.

- (3) Displace fluorocarbon oil at a low rate using the high-pressure displacement system. The core is considered to be saturated with fluorocarbon oil when the liquid production is 5 PV, and measure the  $T_2$  spectrum of the core
- (4) Displace the synthetic formation water at a constant rate using the high-pressure displacement system, and measure its  $T_2$  relaxation time spectrum
- (5) Change the experimental conditions (displacement rate, displacement volume, etc.) and repeat the experimental procedures (1)-(4). It should be noted that injection pressure can be adjusted timely to maintain the constant displacement rate

**2.4. Low-Field Nuclear Magnetic Resonance (NMR).** The decay rate of the NMR signal can be described by the longitudinal relaxation time  $T_1$  and transverse relaxation time  $T_2$ . Because the measurement speed of  $T_2$  is fast, the  $T_2$  measurement method is often used in NMR measurement. The collision between the hydrogen nucleus and the pore wall occurs when the hydrogen nucleus is in transverse relaxation motion, which results in the energy loss of the hydrogen nucleus. The more frequent the collisions, the faster the energy loss of the hydrogen nucleus, thus accelerating the transverse relaxation process of the hydrogen nucleus. The frequency of collision between the hydrogen nucleus and the pore wall is determined by pore size. The larger the pore, the smaller probability the hydrogen nucleus collides with the pore wall, and vice versa. The pore size is inversely proportional to the relaxation rate of hydrogen nuclei, which is the theoretical foundation to investigate pore structure using the NMR spectrum (or  $T_2$  spectrum) [47].  $T_2$  is calculated using the following formula:

$$\frac{1}{T_2} = \frac{1}{T_{2B}} + \frac{1}{T_{2D}} + \frac{1}{T_{2S}}, \quad (1)$$

where  $T_{2B}$  is the relaxation contribution from the fluid itself (i.e., bulk relaxation) with the unit of ms;  $T_{2D}$  is the relaxation contribution from the magnetic gradient diffusion (i.e.,

diffusion relaxation) with the unit of ms; and  $T_{2S}$  is the relaxation contribution from the rock surface (i.e., surface relaxation) with the unit of ms.

When NMR technology is applied to the analysis of tight sandstone cores, the diffusion relaxation can be ignored because it is too small. Therefore, the  $T_2$  relaxation time mainly comes from surface relaxation, followed by bulk relaxation. Surface relaxation is closely related to the specific surface area of tight sandstone cores. The specific surface area of rock refers to the ratio of the pore surface area to the pore volume in rock. The larger the specific surface area, the larger the surface relaxation, the smaller the  $T_2$  relaxation time, and vice versa. Therefore, the  $T_2$  relaxation time of the core can be expressed as

$$\frac{1}{T_2} = \frac{1}{T_{2B}} + \frac{1}{T_{2S}} = \frac{1}{T_{2B}} + \rho \frac{S}{V}, \quad (2)$$

where  $\rho$  is the relaxation rate in  $\mu\text{m}/\text{ms}$  and  $S/V$  is the specific surface area in  $1/\mu\text{m}$ .

Because  $T_{2B}$  is much larger than  $T_2$ ,  $1/T_{2B}$  can be neglected. The relaxation time is mainly from surface relaxation.

$$\frac{S}{V} = \frac{F_S}{r_c}, \quad (3)$$

where  $F_S$  is the shape factor of the single pore (dimensionless) and  $r_c$  is the pore radius in  $\mu\text{m}$ .

By combining Equation (3), Equation (2) can be simplified as

$$T_2 = \frac{r_c}{\rho F_S}. \quad (4)$$

Using  $C = \rho F_S$ , Equation (3) can be transferred as

$$T_2 = C \cdot r_c. \quad (5)$$

It is obvious that the relaxation time  $T_2$  is theoretically a linear function of pore radius  $r_c$ . Therefore, the distribution

of fluids in various pores can be calculated by measuring the signal of the hydrogen nucleus.

### 3. Results and Discussion

*3.1. Effect of Injection Volume on Dynamic Imbibition.* In order to quantitatively evaluate the effect of the injection volume and rate on the dynamic displacement efficiency in tight sandstone, the coefficient  $a$  is given to characterize the increment amplitude of displacement by dynamic imbibition at different injection volumes and rates of formation water, which is the relative displacement efficiency of dynamic imbibition under different injection volumes.

$$a = \frac{V_i}{V_0} \times 100\%, \quad (6)$$

where  $V_0$  is the area of the  $T_2$  spectrum peak of irreducible water in the core and  $V_i$  is the area of the  $T_2$  spectrum peak of formation water under different injection volumes and rates.

The displacement experiments are carried out using synthetic formation water with a 0.1 ml/min displacement rate at different injection volumes. The effects of different injection volumes on the dynamic imbibition displacement of the reservoir core in the target block are evaluated, respectively, as shown in Figures 3–6 and Table 2.

As shown in Figures 3–6 and Table 2, the relative displacement efficiency of core dynamic imbibition increases gradually with the increase of injection volume of synthetic formation water. But the increased amplitude decreases obviously. With the same injection volume, the relative displacement efficiency of core dynamic imbibition increases with the increase of core permeability, especially for core samples No. H-3 and No. H-21, as seen in Figures 3 and 6, respectively.  $T_2$  spectrums present bimodal distribution. For the cores with high permeability, it contains more large pores (including microcracks), and the displacement of dynamic imbibition exhibits the best results at the same injection volume.

For ultralow-permeability reservoirs (permeability lower than 1.0 mD), as shown in Figures 4 and 5 for core samples No. H-7 and No. H-15, when the injection volume is 1.0 PV, the increment amplitudes of relative displacement efficiency of dynamic imbibition reach the maximum values of 30.6% and 49.6%, respectively. When the injection volume increases from 1.0 PV to 1.5 PV, the increment amplitudes of relative displacement efficiency are 18.1% and 21.7%, respectively, with small reductions. When the injection volume increases from 1.5 PV to 2.0 PV, the increased amplitudes of relative displacement efficiency are only 10.5% and 11.3%, respectively, with obvious reductions. When the injection volume increases from 2.0 PV to 2.5 PV, the increment amplitudes of relative displacement efficiency reach the minimum values of only 5.0% and 4.9%, respectively. Therefore, for ultralow-permeability reservoirs with permeability less than 1.0 mD, it is recommended to select an injection volume of 1.5–2.0 PV in the field design of imbibition oil recovery to achieve a high oil recovery.

For conventional low-permeability reservoirs (permeability in the range of 1.0 to 10.0 mD), as shown in Figures 3 and 6, respectively, for core samples No. H-3 and No. H-21, when the injection volume is 1.0 PV, the increased amplitudes of relative displacement efficiency reach high values of 91.7% and 80.3%, respectively. When the injection volume increases from 1.0 PV to 1.5 PV, the increased amplitudes of relative displacement efficiency are only 9.6% and 18.0%, respectively, with obvious reductions. When the injection volume increases from 1.5 PV to 2.0 PV, the increased amplitudes of relative displacement efficiency are as low as only 3.0% and 8.6%, respectively. When the injection volume increases from 2.0 PV to 2.5 PV, the increased amplitudes of relative displacement efficiency are as low as only 1.9% and 3.6%, respectively. Therefore, for tight reservoirs with relatively high permeability, it is recommended to select an injection volume of 1.0–1.5 PV to appropriately reduce the injection volume, so as to minimize the construction cost to the most extent on the basis of ensuring the displacement efficiency of dynamic imbibition.

*3.2. Effect of the Displacement Rate on Dynamic Imbibition.* The dynamic imbibition displacement experiments are carried out with 1.0 PV injection volume at different displacement rates. The effects of different displacement rates on the displacement efficiency of dynamic imbibition in the reservoir core of the target area are evaluated (Figures 7–10). The displacement efficiency under different displacement rates is plotted based on Equation (6), as shown in Figure 11. It can be seen from the experimental results that the relative displacement efficiency of core dynamic imbibition increases and then decreases with the increase of the displacement rate. There exists an optimal displacement rate that achieves the highest relative displacement efficiency of dynamic imbibition. The synergistic effect of capillary pressure and viscous force can achieve the highest displacement efficiency at an optimal displacement rate. When the displacement rate is lower than the optimal displacement rate, capillary pressure plays a dominant role, and crude oil in small pores is easier to be produced. Therefore, it can be seen from Figures 7–10 that the relative displacement efficiency of small pores (left part of the  $T_2$  spectrum) at a low displacement rate is higher than that at a high displacement rate. When the displacement rate is higher than the optimal displacement rate, the differential pressure drive plays a dominant role, and the crude oil in large pores is easier to be produced. Therefore, there exists an optimal displacement rate to displace crude oil in the pores to the most extent. In addition, when the displacement rate is high, the time of the oil-water exchange in the pores is shortened, so that the water in the pores is displaced prematurely, resulting in the decrease of imbibition displacement efficiency. Therefore, it is necessary to select the appropriate injection rate to achieve the best displacement efficiency in the field construction design.

It can be seen from Figure 11 that core samples with high permeability (such as No. H-3 and No. H-21) have higher relative oil displacement efficiency of dynamic imbibition than core samples with low permeability (such as No. H-7

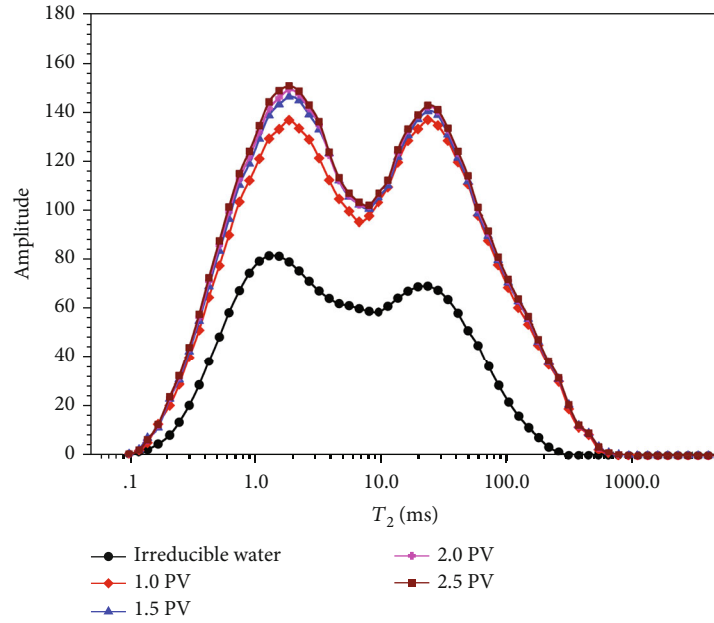


FIGURE 3:  $T_2$  spectrum of the core sample No. H-3 under different injection volumes.

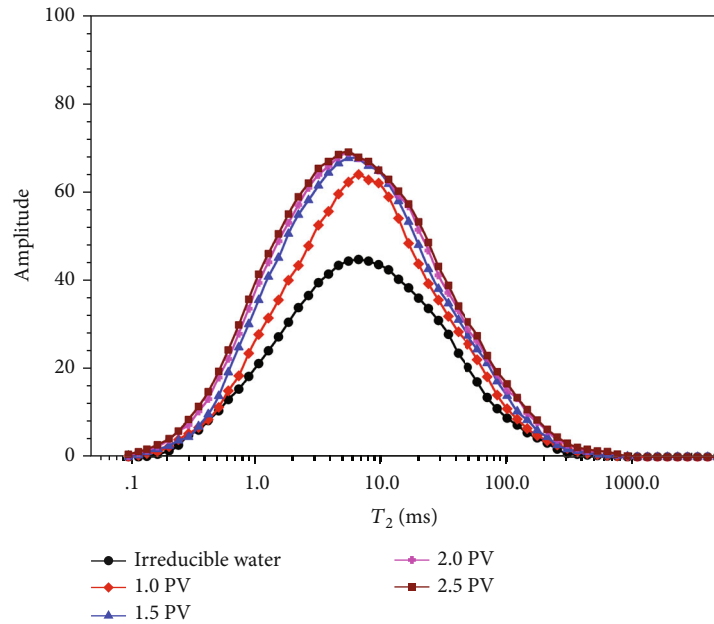


FIGURE 4:  $T_2$  spectrum of the core sample No. H-7 under different injection volumes.

And No. H-15). The high permeability of tight sandstone means that not only there are more large pores but also there might be more microcracks. These microcracks in the tight core can increase the surface area of the core for imbibition and provide more channels for the imbibition, effectively promoting the imbibition. Under the experimental condition of dynamic imbibition, the flowing formation water can timely displace the oil replaced by imbibition from the large pore, improving the imbibition to a certain extent.

It can be seen from Figure 12 that the optimal displacement rate almost linearly increases with the increase of core

permeability. When the reservoir permeabilities are 0.138, 0.281, 1.213, and 2.451 mD, the optimal displacement rates are 0.05, 0.1, 0.2, and 0.4 ml/s, respectively, and the corresponding maximum displacement efficiency of imbibition is 142.2%, 149.6%, 210.2%, and 211.6%, respectively.

The linear correlation between optimal displacement velocity and permeability is regressed as follows:

$$v_{\text{optimal}} = 0.1444K + 0.0401, \quad (7)$$

$$R^2 = 0.9897.$$

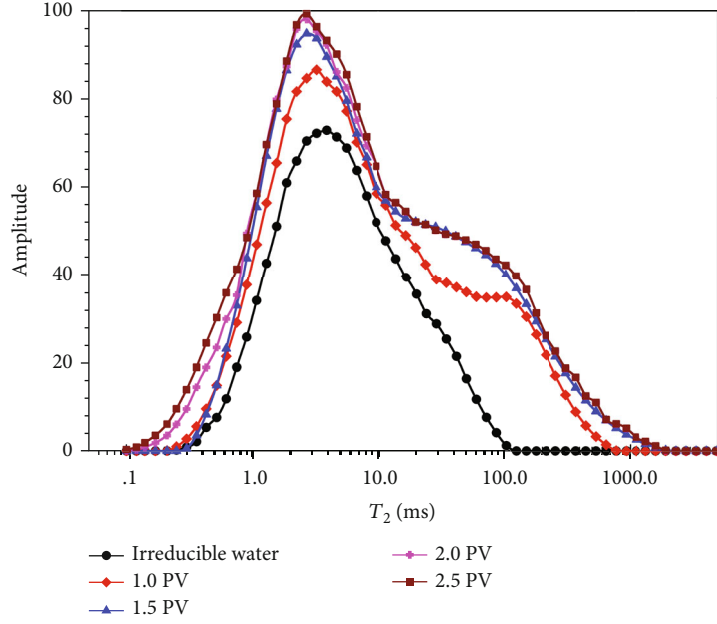


FIGURE 5:  $T_2$  spectrum of the core sample No. H-15 under different injection volumes.

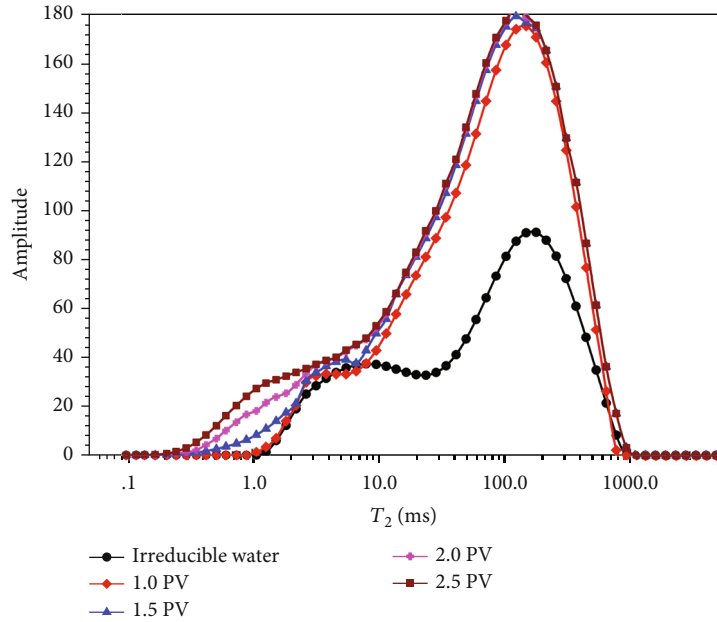


FIGURE 6:  $T_2$  spectrum of the core sample No. H-21 under different injection volumes.

TABLE 2: Dynamic imbibition displacement experiment results under different injection volumes.

Sample no.	Permeability (mD)	1.0 PV (%)	1.5 PV (%)	2.0 PV (%)	2.5 PV (%)
H-3	2.451	191.7	201.3	204.3	206.2
H-7	0.138	130.6	148.7	159.2	164.2
H-15	0.281	149.6	171.3	182.6	187.5
H-21	1.213	180.3	198.3	206.9	210.5

3.3. *Comparison of Static Imbibition and Dynamic Displacement.* From the results in Section 3.2, the relative displacement efficiency of imbibition in small pores is higher at the low displacement rate. Based on this conclusion, the core sample No. H-2 is used to compare and analyze the effects of static imbibition and dynamic imbibition on displacement efficiency in this section. Static imbibition is also referred to as spontaneous imbibition. A nonwetting phase is displaced by a wetting phase in the porous medium only by capillary pressure, without other pressure differences.

The static imbibition experiment is performed with the same experimental equipment in Figure 2. After the synthetic

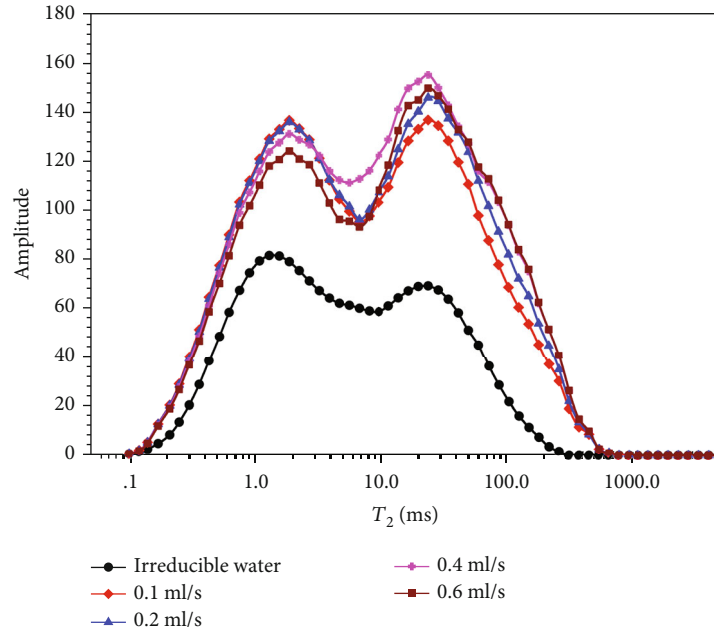


FIGURE 7:  $T_2$  spectrum of the core sample No. H-3 under different displacement rates.

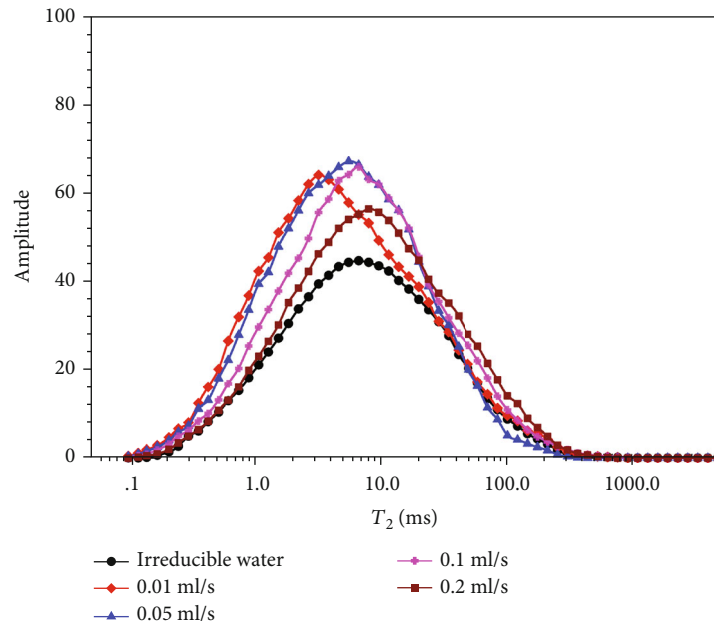


FIGURE 8:  $T_2$  spectrum of the core sample No. H-7 under different displacement rates.

formation water is injected, the valves at the inlet and outlet ends of the core are closed. The core is soaked for a period of time, then the  $T_2$  spectrum is measured. When the soaking time of static imbibition is 24 h, 48 h, and 96 h, the increments of the recovery factor are 172.1%, 206.2%, and 219.1%. The experimental results are shown in Figure 13, in which the experimental conditions of the dynamic imbibition  $T_2$  spectrum are measured at the injection volume of 1 PV and injection rate of 0.2 ml/s.

It can be seen from Figure 13 that the displacement efficiency of static imbibition in small pores is higher than that

of dynamic imbibition. The displacement efficiency of static imbibition increases with the increase of soaking time, but the increased amplitude slows down obviously after reaching a certain time, so the static imbibition also has the optimal imbibition time. However, the displacement efficiency of dynamic imbibition in large pores or microcracks is significantly higher than that of static imbibition. In the process of imbibition, the small pores can provide more forces for imbibition because of the small capillary radius, while the large pores or microcracks can provide an effective channel for the oil replaced by dynamic displacement. It is possible

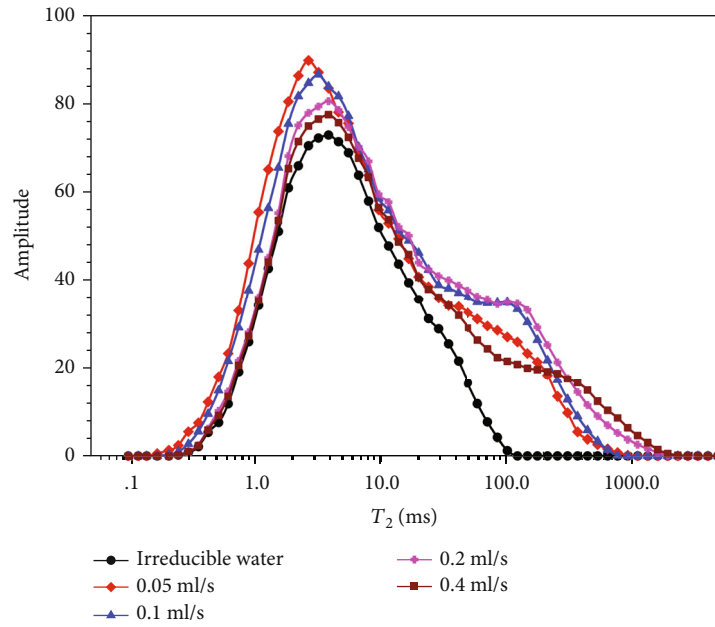


FIGURE 9:  $T_2$  spectrum of the core sample No. H-15 under different displacement rates.

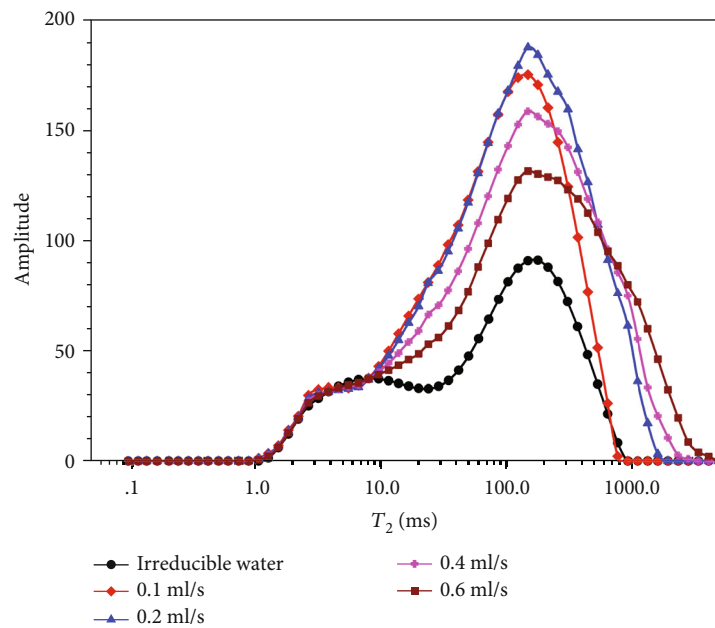


FIGURE 10:  $T_2$  spectrum of the core sample No. H-21 under different displacement rates.

to obtain the highest efficiency of imbibition recovery only when these two aspects are combined effectively.

Therefore, in the actual field process of waterflooding imbibition recovery, the static imbibition and the dynamic imbibition can be combined to achieve a higher recovery efficiency of tight sandstone reservoirs. In field application, a relatively small injection rate is applied to avoid water channeling. The well is then shut in for a while. The shut-in period is determined by laboratory spontaneous imbibition core experiments. An optimal injection rate is carried out based on the conclusions in Section 3.2 to perform dynamic imbibition to improve the final recovery factor.

#### 4. Conclusion

The microdisplacement mechanisms of dynamic imbibition are investigated based on the NMR technique. A set of experiments, including dynamic displacement, spontaneous imbibition, permeability measurements, and scanning electron microscopy, are performed to analyze the effect of displacement volume and displacement velocity on displacement efficiency. Furthermore, the comparison between static imbibition and dynamic imbibition on displacement efficiency is performed. The conclusion can be summarized based on experimental results:

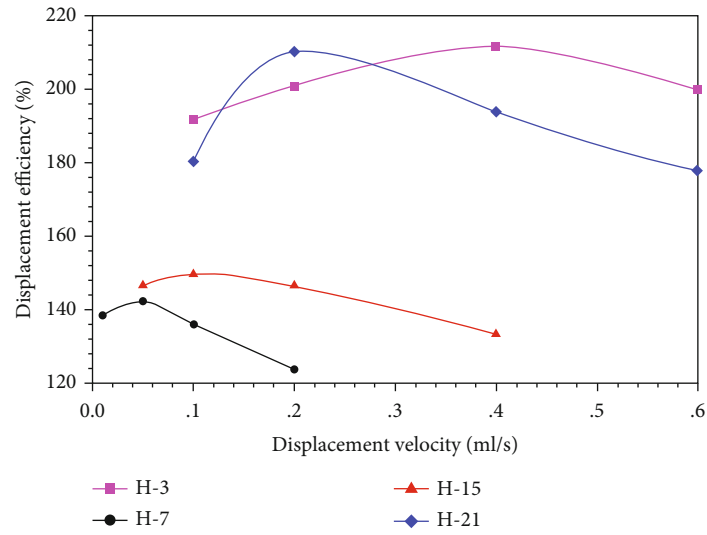


FIGURE 11: Dynamic imbibition displacement efficiency under different displacement rates.

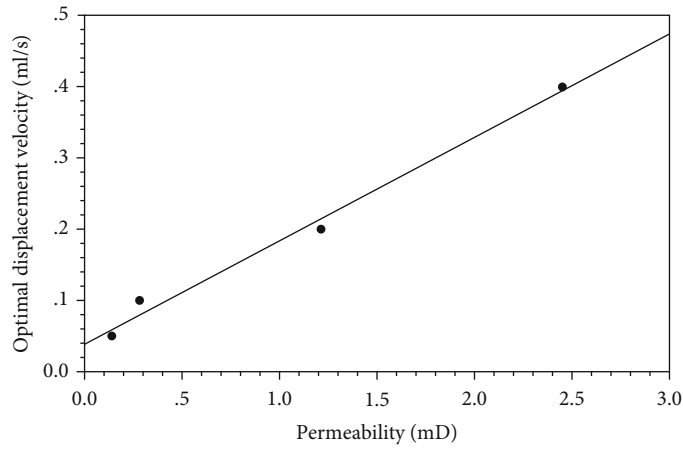


FIGURE 12: Relationship between optimal displacement velocity and permeability.

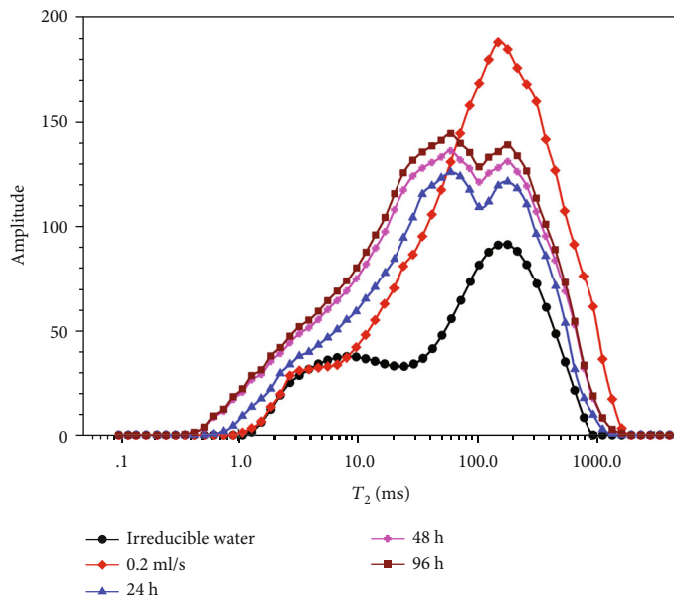


FIGURE 13: Comparison of static imbibition and dynamic displacement.

- (1) The relative displacement efficiency of core dynamic imbibition increases with the increase of injection volume, but the increased amplitude decreases with the increase of injection volume. Under the same injection volume, the relative displacement efficiency of core dynamic imbibition increases significantly with the increase of core permeability. For ultralow-permeability reservoirs with permeability less than 1.0 mD, it is recommended to select an injection volume of 1.5-2.0 PV. For low-permeability reservoirs with permeability greater than 1.0 mD, it is recommended to select an injection volume of 1.0-1.5 PV
- (2) The displacement efficiency of core dynamic imbibition shows a trend of first rising and then declining with the gradual increase of the displacement rate. There exists an optimal displacement rate, under which the synergistic effect of capillary pressure and viscous force can achieve the highest displacement efficiency of dynamic imbibition. The optimal displacement rate almost linearly increases with the increase of core permeability. At a low displacement rate, the relative displacement efficiency in small pores is higher
- (3) The displacement efficiency of static imbibition increases with the increase of soaking time, but the increased amplitude slows down obviously after reaching a certain time. The displacement efficiency of static imbibition in small pores is higher than that of dynamic imbibition. However, the displacement efficiency of dynamic imbibition in large pores or microcracks is significantly higher than that of static imbibition

## Data Availability

All data, models, and code generated or used during the study appear in the article, and the authors are not restricted from sharing their data and materials.

## Conflicts of Interest

The authors declare that they have no conflicts of interest.

## Acknowledgments

This research was financially supported by the National Natural Science Foundation of China (Nos. 52074221 and 51774236), the Foundation of State Key Laboratory of Petroleum Resources and Prospecting, China University of Petroleum, Beijing (No. PRP/open-1703), and the Natural Science Foundation of Shaanxi Province (2019JQ-403).

## References

- [1] T. Jacobs, "Unconventional resources will require unconventional EOR," *Journal of Petroleum Technology*, vol. 67, no. 9, pp. 68-70, 2016.
- [2] Z. Yang, L. H. Hou, S. Z. Tao et al., "Formation conditions and 'sweet spot' evaluation of tight oil and shale oil," *Petroleum Exploration and Development*, vol. 42, pp. 555-565, 2015.
- [3] L. B. Dou, M. Zhang, G. Bi, and T. T. Li, "Transient flow in wellbores and phase transition of CO<sub>2</sub> during formation supercritical CO<sub>2</sub> invasion," *Energy Science & Engineering*, vol. 7, no. 2, pp. 323-337, 2019.
- [4] W. ZHAO, S. HU, L. HOU et al., "Types and resource potential of continental shale oil in China and its boundary with tight oil," *Petroleum Exploration and Development*, vol. 47, no. 1, pp. 1-11, 2020.
- [5] R. G. Loucks, R. M. Reed, S. C. Ruppel, and D. M. Jarvie, "Morphology, genesis, and distribution of nanometer-scale pores in siliceous mudstones of the Mississippian Barnett Shale," *Journal of Sedimentary Research*, vol. 79, no. 12, pp. 848-861, 2009.
- [6] H. N. Philip, "Pore-throat sizes in sandstones, tight sandstones, and shales," *AAPG Bulletin*, vol. 93, pp. 329-340, 2009.
- [7] W. K. Camp, "Pore-throat sizes in sandstones, tight sandstones, and shales: discussion," *AAPG Bulletin*, vol. 95, no. 8, pp. 1443-1447, 2011.
- [8] H. YANG, X. LIANG, X. NIU, S. FENG, and Y. YOU, "Geological conditions for continental tight oil formation and the main controlling factors for the enrichment: a case of Chang 7 Member, Triassic Yanchang Formation, Ordos Basin, NW China," *Petroleum Exploration and Development*, vol. 44, no. 1, pp. 11-19, 2017.
- [9] E. W. Washburn, "The dynamics of capillary flow," *Physical Review*, vol. 17, no. 3, pp. 273-283, 1921.
- [10] L. Handy, "Determination of effective capillary pressures for porous media from imbibition data," *Transactions of the AIME*, vol. 219, no. 1, pp. 75-80, 2013.
- [11] G. Hamon and J. Vidal, "Scaling-up the capillary imbibition process from laboratory experiments on homogeneous and heterogeneous samples," in *European Petroleum Conference*, London, United Kingdom, October 1986.
- [12] G. Mason and N. R. Morrow, "Capillary behavior of a perfectly wetting liquid in irregular triangular tubes," *Journal of Colloid and Interface Science*, vol. 141, no. 1, pp. 262-274, 1991.
- [13] L. Cuiec, B. Bourbiaux, and F. Kalaydjian, "Oil recovery by imbibition in low-permeability chalk," *SPE Formation Evaluation*, vol. 9, pp. 34-52, 1994.
- [14] X. Zhang, N. R. Morrow, and S. Ma, "Experimental verification of a modified scaling group for spontaneous imbibition," *SPE Reservoir Engineering*, vol. 11, no. 4, pp. 280-285, 2013.
- [15] S. X. Ma, X. Y. Zhang, and N. R. Morrow, "Influence of fluid viscosity on mass transfer between fractures and matrix," *Journal of Canadian Petroleum Technology*, vol. 38, pp. 25-30, 1999.
- [16] D. Zhou, L. Jia, J. Kamath, and A. R. Kavscek, "Scaling of counter-current imbibition processes in low-permeability porous media," *Journal of Petroleum Science and Engineering*, vol. 33, no. 1-3, pp. 61-74, 2002.
- [17] M. Ding and M. Kantzas, "Investigation of liquid imbibition mechanisms using NMR," in *Proceedings of the International Symposium of the Society of Core Analysts*, Pau, France, 2003.
- [18] K. Li and R. Horne, "An analytical scaling method for spontaneous imbibition in gas/water/rock systems," *SPE Journal*, vol. 9, pp. 322-329, 2013.
- [19] D. Quere, "Wetting and roughness," *Annual Review of Materials Research*, vol. 38, no. 1, pp. 71-99, 2008.

- [20] N. Fries and M. Dreyer, "An analytic solution of capillary rise restrained by gravity," *Journal of Colloid and Interface Science*, vol. 320, no. 1, pp. 259–263, 2008.
- [21] D. C. Standnes, "Calculation of viscosity scaling groups for spontaneous imbibition of water using average diffusivity coefficients," *Energy & Fuels*, vol. 23, no. 4, pp. 2149–2156, 2009.
- [22] G. Mason, H. Fischer, N. R. Morrow, and D. W. Ruth, "Correlation for the effect of fluid viscosities on counter-current spontaneous imbibition," *Journal of Petroleum Science and Engineering*, vol. 72, no. 1-2, pp. 195–205, 2010.
- [23] K. Schmid and S. Geiger, "Universal scaling of spontaneous imbibition for arbitrary petrophysical properties: water-wet and mixed-wet states and Handy's conjecture," *Journal of Petroleum Science and Engineering*, vol. 101, pp. 44–61, 2013.
- [24] S. Strand, D. Standnes, and T. Austad, "Spontaneous imbibition of aqueous surfactant solutions into neutral to oil-wet carbonate cores: effects of brine salinity and composition," *Energy & Fuels*, vol. 17, no. 5, pp. 1133–1144, 2003.
- [25] L. Sun, W. F. Pu, J. Xin, and Y. L. Wu, "Influence of surfactant on high temperature imbibition of low permeability cores," *Journal of China University of Petroleum*, vol. 36, pp. 103–107, 2012.
- [26] Z. Y. Qi, M. Han, A. Fuseni et al., "Laboratory study on surfactant induced spontaneous imbibition for carbonate reservoir," in *SPE Asia Pacific Oil & Gas Conference and Exhibition*, Perth, Australia, October 2016.
- [27] J. O. Alvarez and D. S. Schechter, "Wettability alteration and spontaneous imbibition in unconventional liquid reservoirs by surfactant additives," *SPE Reservoir Evaluation & Engineering*, vol. 20, no. 1, pp. 107–117, 2017.
- [28] C. L. Dai, R. Cheng, X. Sun et al., "Oil migration in nanometer to micrometer sized pores of tight oil sandstone during dynamic surfactant imbibition with online NMR," *Fuel*, vol. 245, pp. 544–553, 2019.
- [29] U. Kuila, D. K. McCarty, A. Derkowski, T. B. Fischer, T. Topór, and M. Prasad, "Nano-scale texture and porosity of organic matter and clay minerals in organic-rich mudrocks," *Fuel*, vol. 135, pp. 359–373, 2014.
- [30] S. Takahashi and A. R. Kovscek, "Spontaneous countercurrent imbibition and forced displacement characteristics of low-permeability, siliceous shale rocks," *Journal of Petroleum Science and Engineering*, vol. 71, no. 1-2, pp. 47–55, 2010.
- [31] D. M. Wang, R. Butler, J. Zhang, and R. Seright, "Wettability survey in Bakken shale with surfactant formulation imbibition," *SPE Reservoir Evaluation & Engineering*, vol. 15, pp. 695–705, 2013.
- [32] Z. Zhou, H. Abass, X. Li, D. Beringer, and W. Frank, "Mechanisms of imbibition during hydraulic fracturing in shale formations," *Journal of Petroleum Science and Engineering*, vol. 141, pp. 125–132, 2016.
- [33] J. R. Liu, J. Sheng, X. K. Wang, H. K. Ge, and E. Yao, "Experimental study of wettability alteration and spontaneous imbibition in Chinese shale oil reservoirs using anionic and nonionic surfactants," *Journal of Petroleum Science and Engineering*, vol. 175, pp. 624–633, 2019.
- [34] A. M. Neves, V. C. Santanna, J. L. M. Barillas, T. N. Castro Dantas, and A. G. B. Góis, "Ionic surfactants applied in enhanced oil recovery: adsorption, imbibition, and zeta potential approaches," *Brazilian Journal of Chemical Engineering*, vol. 37, no. 1, pp. 263–269, 2020.
- [35] C. C. Mattax and J. R. Kyte, "Imbibition oil recovery from fractured, water-drive reservoir," *Society of Petroleum Engineers Journal*, vol. 2, pp. 177–184, 2013.
- [36] J. Kleppe and R. A. Morse, "Oil production from fractured reservoirs by water displacement," in *Fall Meeting of the Society of Petroleum Engineers of AIME*, Houston, Texas, 1974.
- [37] M. Pooladi-Darvish and A. Firoozabadi, "Experiments and modelling of water injection in water-wet fractured porous media," in *Annual Technical Meeting*, Calgary, Alberta, 1998.
- [38] G. C. Tzimas, T. Matsuura, D. G. Avraam, W. van der Bruggen, G. N. Constantinides, and A. C. Payatakes, "The combined effect of the viscosity ratio and the wettability during forced imbibition through nonplanar porous media," *Journal of Colloid and Interface Science*, vol. 189, no. 1, pp. 27–36, 1997.
- [39] A. Graue, T. Bognø, B. A. Baldwin, and E. A. Spinler, "Wettability effects on oil-recovery mechanisms in fractured reservoirs," *SPE Reservoir Evaluation & Engineering*, vol. 4, pp. 455–466, 2013.
- [40] G. Q. Tang and A. Firoozabadi, "Effect of pressure gradient and initial water saturation on water injection in water-wet and mixed-wet fractured porous media," *SPE Reservoir Evaluation & Engineering*, vol. 4, pp. 516–524, 2013.
- [41] A. A. Al-Quraishi, "Oil recovery by dynamic imbibition in low tension aqueous systems," *Oil & Gas Science and Technology*, vol. 59, no. 3, pp. 267–273, 2004.
- [42] E. Hamidpour, A. Mirzaei-Paiaman, M. Masihi, and B. Harimi, "Experimental study of some important factors on nonwetting phase recovery by cocurrent spontaneous imbibition," *Journal of Natural Gas Science and Engineering*, vol. 27, pp. 1213–1228, 2015.
- [43] P. S. Hammond and E. Unsal, "Spontaneous and forced imbibition of aqueous wettability altering surfactant solution into an initially oil-wet capillary," *Langmuir*, vol. 25, no. 21, pp. 12591–12603, 2009.
- [44] J. Sharma, S. B. Inwood, and A. R. Kovscek, "Experiments and analysis of multiscale viscous fingering during forced imbibition," *SPE Journal*, vol. 17, pp. 1142–1159, 2013.
- [45] Y. Qiao, P. Ø. Andersen, S. Evje, and D. C. Standnes, "A mixture theory approach to model co- and counter-current two-phase flow in porous media accounting for viscous coupling," *Advances in Water Resources*, vol. 112, pp. 170–188, 2018.
- [46] P. Ø. Andersen, Y. Qiao, D. C. Standnes, and S. Evje, "Cocurrent spontaneous imbibition in porous media with the dynamics of viscous coupling and capillary backpressure," *SPE Journal*, vol. 24, no. 1, pp. 158–177, 2019.
- [47] H. Gao, C. Wang, J. Cao, M. Q. He, and L. B. Dou, "Quantitative study on the stress sensitivity of pores in tight sandstone reservoirs of Ordos basin using NMR technique," *Journal of Petroleum Science and Engineering*, vol. 172, pp. 401–410, 2019.